https://doi.org/10.5194/egusphere-2023-2698
Preprint. Discussion started: 6 December 2023
© Author(s) 2023. CC BY 4.0 License.

Daytime and nighttime aerosol soluble iron formation in clean and slightly-polluted moisture air in a coastal city in eastern China

Wenshuai Li[1,2], Yuxuan Qi[1,2], Yingchen Liu[1,2], Guanru Wu[1,2], Yanjing Zhang[1,2], Jinhui Shi[3], Wenjun Qu[1,2], Lifang Sheng[1,2], Wencai Wang[1,2], Daizhou Zhang[4], Yang Zhou[1,2]

[1]Frontier Science Center for Deep Ocean Multispheres and Earth System (FDOMES) and Physical Oceanography Laboratory, Ocean University of China, Qingdao 266100, China.

[2]College of Oceanic and Atmospheric Sciences, Ocean University of China, Qingdao 266100, China.

[3]College of Environmental Science and Engineering, Ocean University of China, Qingdao 266100, China.

[4]Faculty of Environmental and Symbiotic Sciences, Prefectural University of Kumamoto, Kumamoto 862-8502, Japan.

Correspondence to: Daizhou Zhang (dzzhang@pu-kumamoto.ac.jp) and Yang Zhou (yangzhou@ouc.edu.cn)

Abstract. Photocatalysis reactions occurring during daytime and aqueous-phase reactions during both daytime and nighttime constitute the two primary processes responsible for converting aerosol iron (Fe) from insoluble to soluble forms within the atmosphere. This study investigated the composition of total Fe (Fe_T) and soluble Fe (Fe_S) in daytime and nighttime $PM_{2.5}$ in Qingdao, a coastal city in eastern China, and evaluated the distinctive roles of the two pathways in enhancing the solubility of aerosol Fe (%Fe_S, the ratio of Fe_S to Fe_T). In clean and humid conditions characterized by sea breezes, with relative humidity (RH) prevalently exceeding 80%, an average daytime %Fe_S of 8.7% was observed, which systematically surpassed its nighttime %Fe_S (6.3%). In contrast, when the air originated from land regions and was slightly polluted, the daytime %Fe_S (3.7%) was noted to be lower than the nighttime %Fe_S (5.8%). This discrepancy was attributable to the variations in RH, as the nighttime RH approximated to be 77%, facilitating the more efficient formation of acidic substances and resulting in faster Fe_S production than during daytime, when RH was about 62%. Furthermore, the oxidation rates of sulfur (SOR) and nitrogen (NOR) displayed strong correlations with RH, particularly when RH was below 75%. A 10% increase in RH resulted in a 7.6% increase in SOR and a 7.2% elevation in NOR, which served as the primary reason for the differences in aerosol acidity and %Fe_S between daytime and nighttime. These findings highlight the RH-dependent activation of aqueous-phase reactions and the augmentation of daytime photocatalysis in the formation of Fe_S in the coastal moisture atmosphere.

https://doi.org/10.5194/egusphere-2023-2698
Preprint. Discussion started: 6 December 2023
© Author(s) 2023. CC BY 4.0 License.

1 Introduction

Iron (Fe) in atmospheric aerosol particles plays a crucial role as a micronutrient in marine ecosystems (Martin et al., 1994). Its deposition to open oceans can stimulate phytoplankton boom, and ultimately enhance the absorption and fixation of atmospheric carbon in seawater (Watson et al., 1994; Watson and Lefévre, 1999). Studies have shown that only the soluble part of Fe (Fe_S) in aerosols is available to the phytoplankton, namely bioavailable Fe (Zhuang et al., 1992; Sugie et al., 2013). The fraction of Fe_S in total aerosol Fe (Fe_T), i.e., the aerosol Fe solubility (%Fe_S), depends on the sources of the aerosols and the chemical conversions of Fe from insoluble forms to soluble forms in the atmosphere. The %Fe_S in nascent dust particles is typically less than 1%, while it can exceed 10% in combustion-derived aerosols (e.g., coal and oil combustion fly ash) (Oakes et al., 2012; Shi et al., 2012; Wang et al., 2015; Li et al., 2022). The %Fe_S in primary particles can be significantly enlarged through atmospheric conversions, which is the consequence of aerosol acidification mainly via aqueous-phase reactions or absorption from the air (Solmon et al., 2009; Shi et al., 2015; Hettiarachchi et al., 2019). These conversions have been found to sway the deposition flux of aerosol Fe_S over the open ocean (Chen and Siefert, 2004; Shi et al., 2013; Yang et al., 2020).

Solar radiation and ambient humidity are two key meteorological factors that greatly influence the processes of aerosol acidification. During daylight hours, solar irradiation triggers photochemical reactions that generate free radicals and accelerate the formation of acidic species in aerosol particles, facilitating the dissolution of aerosol Fe (Chen and Grassian, 2013; Liu et al., 2021b). Fu et al. (2010) observed a noteworthy increase of Fe_S in dust samples upon light exposure in the HCl solution. Daytime photolysis of Fe-organic complexes also results in the production of Fe_S, contributing to the rise in %Fe_S (Weller et al., 2014; Zhang et al., 2019; Zhou et al., 2020). For instance, Zhou et al. (2020) and Zhang et al. (2019) found that the oxalate−Fe(III) photolysis can result in the degradation of oxalate and facilitate the Fe dissolution in aerosol particles during daytime. Relevant mechanisms were determined in lab experiments and model simulations (Zhu et al., 1993; Chen and Grassian, 2013; Sorooshian et al., 2013; Pang et al., 2019; Li et al., 2021). In contrast, high ambient relative humidity (RH) can trigger robust heterogeneous/liquid phase formation of sulfate and nitrate during nighttime, intensifying aerosol acidity and activating acids-associated dissolution of Fe (Liu et al., 2020; Pye et al., 2020; Wong et al., 2020). Zhang et al. (2022) investigated the solubility of aerosol iron in winter in the city of this study and found enhanced %Fe_S (>1%) at high RH (>60%). Zhu et al. (2020) asserted that sulfates/nitrates had stronger effects on %Fe_S at RH>50%

https://doi.org/10.5194/egusphere-2023-2698
Preprint. Discussion started: 6 December 2023
© Author(s) 2023. CC BY 4.0 License.

compared to RH<50%. Shi et al. (2020) observed the efficient production of Fe_S in fog processes, where SO_4^{2-} and NO_3^- abounded due to the absorption of precursor gases on wet surfaces of particles, enabling particles to absorb more water vapor, and resulting in the increase of Fe_S consequently.

Aqueous-phase conversion can occur during both daytime and nighttime when there is sufficient moisture. The formation of Fe_S is the consequence of the combination of photochemistry and aqueous chemistry during daytime, while it is solely dependent on aqueous chemistry at night. The collaborative mechanisms between photochemistry and aqueous chemistry in Fe_S formation, as well as their respective contributions, are still inadequately comprehended.

To study the roles of aqueous-phase reactions and photochemical reactions on Fe_S formation, we collected $PM_{2.5}$ samples during daytime and nighttime, separately, in a Chinese coastal city (Qingdao). Qingdao is situated under the westerlies of the Northern Hemisphere, serving as the primary pathway for the transport of Fe_S from East Asia to the Northwestern Pacific. We focused on studying the enhancement of $\%Fe_S$ under clean and slightly-polluted air conditions—the most common states of air pollution in coastal regions. Our investigation aimed to understand how aqueous-phase reactions and photochemical reactions contribute to aerosol $\%Fe_S$ enhancement.

2 Methodology and materials

2.1 Sample collection and classification

The observation was carried out on the following dates: April 24th to May 27th, 2017; March 28th to April 30th, 2018; and May 22nd to 28th, 2018. Two high-volume $PM_{2.5}$ samplers (TISCH, TE-6070BLX-2.5, USA) were applied to collect $PM_{2.5}$ onto quartz microfiber filters (QM-A, PALL) and Whatman® 41 filters, respectively, on the roof of Baguanshan Atmospheric Research Observatory (BARO, 36°03' N, 120°20' E, 76 m asl.). BARO is located on the top of a small hill in the urban area of Qingdao, and approximately 0.7 km away from the coastline of the Yellow Sea (Figure S1). $PM_{2.5}$ samples were collected separately during daytime and nighttime. Field blank samples were also collected during the campaign by placing filters in the samplers with the samplers switched off. Following the sampling process, $PM_{2.5}$ samples were sealed and stored at −20°C before analysis.

For the measurement of water-soluble ions (WSIs) and carbonaceous matters, aerosol samples collected on QM-A filters were utilized. The samples collected on Whatman® 41 filters were used for the detection of elements. First, samples were cut into pieces and immersed in Milli-Q pure water. Then, water-soluble matters were extracted by ultrasonic vibration at approximately 0°C for 40 min. The water extracts were then filtered through syringes

https://doi.org/10.5194/egusphere-2023-2698
Preprint. Discussion started: 6 December 2023
© Author(s) 2023. CC BY 4.0 License.

with 0.45 μm strainer heads (PALL). The filtered extracts were analyzed for WSIs, including Na^+, NH_4^+, K^+, Mg^{2+}, Ca^{2+}, F^-, Cl^-, SO_4^{2-}, NO_3^-, $C_2O_4^{2-}$, using ion chromatography (IC, Dionex ICS-3000, Dionex Corp., Sunnyvale, CA, USA). Sample pretreatment procedures used to determine soluble elements were similar. While, 10 ml filtrate was taken and 0.187 ml HNO_3 (mass fraction: 69%) was added into water extracts before the measurement of soluble elements in case soluble Fe(II) was oxidized into the insoluble state. To determine total elements, sample pieces were placed into inner-tanks and subjected to digestion with a mixture of HNO_3 + HF (at a volume ratio of 4:1) at 180°C for 48 h. The element concentrations were measured using inductively coupled plasma mass spectrometry (ICP-MS, Model: iCAP Qc, Thermo Fisher Scientific Inc., Germany). Carbonaceous materials, specifically organic carbon (OC) and elemental carbon (EC), were analyzed using a sunset OC/EC analyzer from Sunset Laboratory Inc. The detection limits of the analysis instruments used can be found in Table S1. The organic matter (OM) content was estimated with 1.6 times OC, as proposed by Turpin and Lim (2001). Further details about sample collection, pretreatment procedures, and chemical species detection can be found in our previous work (Li et al., 2023a; Li et al., 2023b).

Various weather conditions and air pollution characteristics were encountered during the observation period, including clean, slightly-polluted (SP), heavily-polluted, foggy, and dusty conditions. Due to the large deviations and uncertainties in the statistical results of dust-related samples, data from these samples were not considered. Additionally, samples from heavily-polluted periods (N = 6, defined by $PM_{2.5} > 50$ μg m^{-3} and $PM_{2.5}/PM_{10} > 0.4$) and fog-influenced samples (N = 12) were not included, either, because of the limited sample number and the significant difference of fog durations between samples. In this paper, we focus on the results of the clean period samples (N = 19) and the SP period samples (N = 32). Clean periods samples were collected when $PM_{2.5} < 30$ μg m^{-3} and $PM_{10} < 50$ μg m^{-3}. The SP periods samples were those collected when 30 μg $m^{-3} < PM_{2.5} < 50$ μg m^{-3} and those collected when $PM_{2.5} < 30$ μg m^{-3} while $PM_{10} > 50$ μg m^{-3}.

2.2 Aerosol pH and liquid water content

ISORROPIA (version II) thermodynamic equilibrium model was employed to estimate gas concentrations and aerosol water pH (Song et al., 2018). The forward mode, which uses both gas and aerosol data as model input, was utilized for pH calculations. This approach was favored over the reverse mode because the reverse mode with only aerosol data is very sensitive to the uncertainties of the measured WSIs concentrations (Hennigan et al., 2015; Song et al., 2018). The concentrations of gaseous species were not measured at the observational site. Therefore,

https://doi.org/10.5194/egusphere-2023-2698
Preprint. Discussion started: 6 December 2023
© Author(s) 2023. CC BY 4.0 License.

the concentrations of aerosol components were initially inputted as the sum of aerosol and gas concentrations during the first run, e.g., $[NO_3^- + HNO_3]_{total} = [NO_3^-]_{aerosol}$. Then, the calculated gas concentrations and the aerosol components were utilized as input for a second run, following the methodology outlined by Sun et al. (2018) and Li et al. (2023b). "Metastable-mode" was used in ISORROPIA, assuming that solid precipitates did not form except for $CaSO_4$. The aerosol pH was calculated by employing aqueous H^+ concentration and aerosol liquid water content (ALWC) outputted by ISORROPIA, as described by equation (1).

$$pH = -\log_{10}\frac{1000 \times H^+(aq)}{ALWC} \quad (1)$$

Significant correlations between the results of the first run and the second run results were observed for pH (r^2 = 0.999) and ALWC (r^2 = 0.928), indicating the stability and reliability in estimating the pH and ALWC by the ISORROPIA model.

2.3 Weather conditions and air quality data

The publicly released temperature, RH, surface pressure, wind speed, and wind direction recorded every 10 minutes were obtained from a meteorological observatory of the Qingdao Meteorological Bureau (Figure S1). Hourly mass concentrations of $PM_{2.5}$, PM_{10}, SO_2, NO_2, O_3 and CO were obtained from an adjacent air quality monitoring station in the Shinan District of Qingdao City (Figure S1), which is managed by Ministry of Ecology and Environment of the People's Republic of China (http://www.mee.gov.cn/).

To examine the relative abundance of chemical species in aerosols, we reconstructed the mass concentrations of $PM_{2.5}$ by equation (2) using the obtained concentrations of WSIs, OM, EC and elements.

$$PM_{2.5R} = WSIs + OM + EC + Elements + Si + Ca \quad (2)$$

where $PM_{2.5R}$ is the reconstructed $PM_{2.5}$, and WSIs consists of Na^+, NH_4^+, K^+, F^-, Cl^-, SO_4^{2-}, NO_3^- and $C_2O_4^{2-}$. As for elements, Mg, Al, V, Cr, Mn, Fe, Ni, Co, Cu, Zn, Ga, As, Se, Rb, Sr, Cd, Ba, Tl and Pb were considered. Si and Ca concentrations were estimated based on the mass ratio of Si/Al (3.43) following the methodology described by Huang et al. (2010) and the mass ratio of Ca/Al (0.80) suggested by Arimoto et al. (2004) and Wang et al. (2011).

2.4 Provenances of air masses

The HYbrid Single-particle Lagrangian Integrated Trajectory (HYSPLIT) Model (https://www.ready.noaa.gov/HYSPLIT.php), developed by NOAA, was applied to calculate the origins of air

https://doi.org/10.5194/egusphere-2023-2698
Preprint. Discussion started: 6 December 2023
© Author(s) 2023. CC BY 4.0 License.

masses from which $PM_{2.5}$ samples were collected. Gridded GDAS data with a horizontal resolution of 1.0° × 1.0° were used as the input. Backward trajectories were computed for a period of 48 hours, with starting points located at 300 meters above ground level.

3 Results

3.1 Meteorological features of clean and SP periods

During clean periods, the backward trajectories demonstrate that the air masses primarily originated from sea areas (Figure 1). The prevailing sea breeze resulted in high RH levels of 81.5 ± 4.9% during daytime and 86.6 ± 8.8% during nighttime (Table 1). The small temperature difference of less than 2℃ between daytime and nighttime further reflects the characteristics of oceanic air. In contrast, air masses during SP periods originated from various directions and most of them passed land areas before reaching the sampling site. Temperature and RH exhibited noticeable diurnal variations. The daytime temperature was 17.2 ± 3.0℃ and decreased to 13.2 ± 3.7℃ during nighttime. The RH levels were 62.1 ± 9.4% and 76.8 ± 9.4% during daytime and nighttime, respectively.

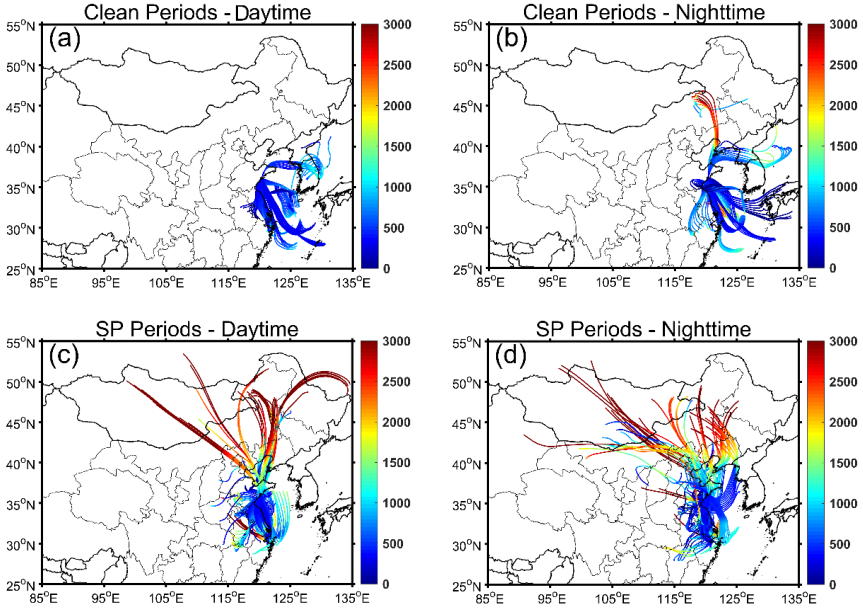

Figure 1: 48-h backward trajectories during daytime and nighttime during clean and slightly-polluted (SP) periods. Trajectories are color-coded based on the altitude (unit: m) above the ground.

https://doi.org/10.5194/egusphere-2023-2698
Preprint. Discussion started: 6 December 2023
© Author(s) 2023. CC BY 4.0 License.

Table 1. Meteorological parameters, %Fe_S, aerosol pH, the concentrations (average ± standard deviation) of $PM_{2.5}$ and chemical species during clean and slightly-polluted periods.

	Clean Periods		Slightly-polluted Periods	
	Daytime	Nighttime	Daytime	Nighttime
$PM_{2.5}$ (μg m^{-3})	16.9 ± 3.1	16.4 ± 5.6	30.3 ± 7.0	28.3 ± 7.7
Temperature (°C)	16.6 ± 2.8	14.3 ± 2.3	17.2 ± 3.0	13.2 ± 3.7
RH (%)	81.5 ± 4.9	86.6 ± 8.8	62.1 ± 9.4	76.8 ± 9.4
ALWC (μg m^{-3})	30.0 ± 13.6	52.0 ± 51.9	22.6 ± 13.5	45.1 ± 34.1
Fe_T (ng m^{-3})	289.2 ± 223.4	186.7 ± 122.2	938.3 ± 850.5	520.3 ± 496.1
Fe_S (ng m^{-3})	20.0 ± 10.5	12.5 ± 7.4	25.7 ± 10.5	21.6 ± 8.1
%Fe_S (%)	8.7 ± 3.8	6.3 ± 4.1	3.7 ± 2.0	5.8 ± 3.0
pH	0.54 ± 0.81	1.20 ± 0.89	1.35 ± 0.91	1.19 ± 0.71
SO_4^{2-} (μg m^{-3})	13.97 ± 5.19	10.97 ± 8.06	14.94 ± 5.81	13.78 ± 5.43
NO_3^- (μg m^{-3})	5.82 ± 3.49	5.63 ± 4.87	26.71 ± 13.15	22.80 ± 10.81
$(2[SO_4^{2-}]+[NO_3^-])/Re\_PM_{2.5}$ (μmol $μg^{-1}$)	0.0115 ± 0.0026	0.0105 ± 0.0023	0.0101 ± 0.0017	0.0106 ± 0.0016

3.2 Concentrations of $PM_{2.5}$ and Fe, and %Fes

Table 1 presents the levels of $PM_{2.5}$ and aerosol Fe concentrations during both clean and SP periods. Under clean conditions, $PM_{2.5}$ concentrations were similar during daytime and nighttime, with average values of 16.9 μg m^{-3} and 16.4 μg m^{-3}, respectively. Compared to the nighttime, both Fe_T and Fe_S concentrations were higher during daytime, indicating more degraded air conditions. Fe_T concentrations were 289.2 ± 223.4 ng m^{-3} during daytime and 186.7 ± 122.2 ng m^{-3} during nighttime. Fe_S concentrations were 20.0 ± 10.5 ng m^{-3} during daytime and 12.5 ± 7.4 ng m^{-3} during nighttime. %Fe_S values ranged from 2.3% to 14.1% with an average of 8.7% ± 3.8% during daytime, which was approximately 1.4 times that during nighttime (6.3% ± 4.1%, after removing an extreme point of 37.2%).

Under SP conditions, $PM_{2.5}$ was at similar levels during daytime and nighttime with the average values of 30.3 μg m^{-3} and 28.3 μg m^{-3}, respectively. However, the daytime Fe_T (938.3 ± 850.5 ng m^{-3}) was much higher than the nighttime Fe_T (520.3 ± 496.1 ng m^{-3}), approximately 3 times higher than during the clean period. Similarly, the daytime Fe_S concentration of 25.7 ± 10.5 ng m^{-3} was slightly higher than the nighttime concentration of 21.6 ± 8.1 ng m^{-3}, which was 1–2 times higher than that during the clean period. Different from the clean period, %Fe_S was

https://doi.org/10.5194/egusphere-2023-2698
Preprint. Discussion started: 6 December 2023
© Author(s) 2023. CC BY 4.0 License.

markedly higher at night (5.8% ± 3.0%) compared to the daytime $\%Fe_S$ (3.7% ± 2.0%) during the SP period, ranging from 1.0% to 12.3%.

3.3 Chemical characteristics of $PM_{2.5}$

Figure 2 illustrates the mass fractions of chemical species present in the reconstructed $PM_{2.5}$ ($PM_{2.5R}$). During the clean period, WSIs were the dominant components, constituting approximately 75.0% and 74.1% of $PM_{2.5}$ during daytime and nighttime, respectively. SO_4^{2-}, NO_3^-, and NH_4^+ were the main contributors to WSIs. In the daytime, SO_4^{2-} and NO_3^- served as the major acid species were 13.97 ± 5.19 μg m^{-3} and 5.82 ± 3.49 μg m^{-3}, respectively, accounting for 43.0% and 15.8% of the $PM_{2.5}$ mass (Table 1 and Figure 2). At night, SO_4^{2-} and NO_3^- concentrations decreased slightly, which were 10.97 ± 8.06 μg m^{-3} and 5.63 ± 4.87 μg m^{-3}, respectively, accounting for 36.8% and 17.7% of $PM_{2.5}$ mass (Table 1 and Figure 2). In other words, the two main acid species, SO_4^{2-} and NO_3^-, had little higher fractions in $PM_{2.5}$ during daytime (58.7%) compared to the nighttime (54.6%), along with the lower ALWC, resulting in the lower aerosol pH of 0.54 ± 0.81 during daytime (Table 1). At night, aerosol pH (1.20 ± 0.89) increased by a factor of 2.2 compared to daytime. We used the ratio of acids to PM, i.e., $(2[SO_4^{2-}]+[NO_3^-])/PM_{2.5R}$, to assess the relative content of acids in unit PM mass and further reveal the aerosol acidity. It was 0.0115 ± 0.0026 μmol μg^{-1} and 0.0105 ± 0.0023 μmol μg^{-1} in $PM_{2.5}$ mass during daytime and nighttime, respectively (Table 1).

During the SP period, WSIs maintained similar proportions in $PM_{2.5}$ as during the clean period, accounting for 70.5% and 74.3% during daytime and nighttime, respectively. SO_4^{2-}, NO_3^-, and NH_4^+ were also the main contributors to WSIs. In the daytime, the concentrations of SO_4^{2-} and NO_3^- were 14.94 ± 5.81 μg m^{-3} and 26.71 ± 13.15 μg m^{-3}, respectively, slightly higher than the nighttime concentrations (Table 1). However, SO_4^{2-} had evidently lower contributions to $PM_{2.5}$ compared to the clean period, which were only 20.9% and 23.0% during daytime and nighttime, respectively. In contrast, NO_3^- had a noticeably higher contribution to $PM_{2.5}$ compared to the clean period, with fractions of 35.4% and 35.6% during daytime and nighttime, respectively. In total, the ratio of acids to PM (i.e., $(2[SO_4^{2-}]+[NO_3^-])/PM_{2.5R}$) was 0.0101 ± 0.0017 μmol μg^{-1} during daytime and 0.0106 ± 0.0016 μmol μg^{-1} during nighttime (Table 1). Even though the ALWC (45.1 ± 34.1 μg m^{-3}) abounded more significantly at night compared to that during daytime (22.6 ± 13.5 μg m^{-3}), the aerosol pH was lower at night. Specifically, the nighttime aerosol pH was 1.19 ± 0.71, while the daytime aerosol pH was slightly higher at 1.35

https://doi.org/10.5194/egusphere-2023-2698
Preprint. Discussion started: 6 December 2023
© Author(s) 2023. CC BY 4.0 License.

± 0.91, indicating weaker aerosol acidity during daytime with a 13.4% increase in pH compared to nighttime aerosols.

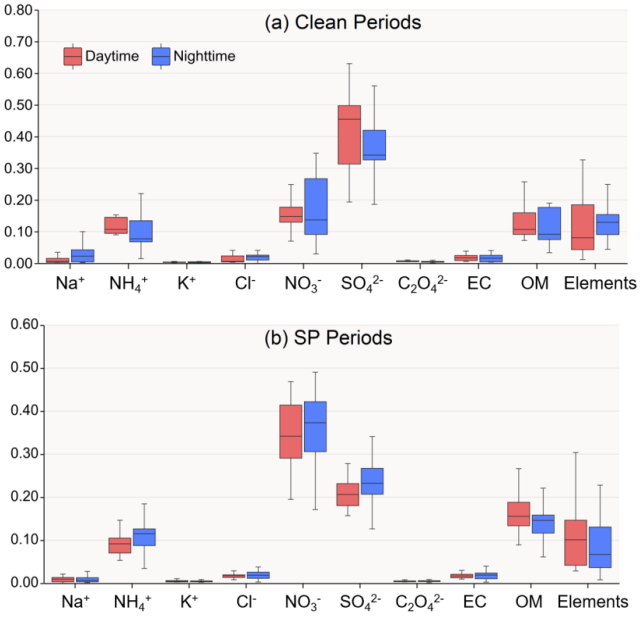

Figure 2: Mass fractions of chemical species in reconstructed $PM_{2.5}$ mass during daytime and nighttime in clean and SP conditions. Mg^{2+} and Ca^{2+} are not shown in the above pictures, because total Mg is included in elements data and total Ca is assessed by 0.8 times Al.

4 Discussion

We found that daytime $\%Fe_S$ was much higher than nighttime $\%Fe_S$ during the clean period, and vice versa during the SP period. Here, the main factors causing the distinct diurnal variation of $\%Fe_S$ during clean and SP periods were discussed, based on the aspects of aqueous-phase conversions and photocatalysis reactions.

4.1 Aqueous-phase conversions promoted by acid processes

The $\%Fe_S$ was dependent on the acidification of the aerosol particles, and high $\%Fe_S$ was associated with low aerosol pH (Table 1). The pH of aerosols is controlled by ALWC and H^+ contents. The predominant acidic species, i.e., SO_4^{2-} and NO_3^-, play crucial roles in promoting the dissolution of insoluble Fe through proton-promoted reactions. As shown in Figure 3a, there was a significant negative correlation between the aerosol pH and the relative content of these two acidic species when the pH was below 4 (r = 0.64). The slope of the regression line

https://doi.org/10.5194/egusphere-2023-2698
Preprint. Discussion started: 6 December 2023
© Author(s) 2023. CC BY 4.0 License.

was about –550.1, indicating that even a minor variation (e.g., 1.0 nmol μg^{-1}) of the acidic species content in $PM_{2.5}$ can lead to a noticeable fluctuation of aerosol pH (about 0.55). For instance, the daytime aerosol pH during the clean period was about 0.66 lower than that of the nighttime during the SP period, even though the difference of the two acidic species content was only about 0.9 ng μg^{-1}.

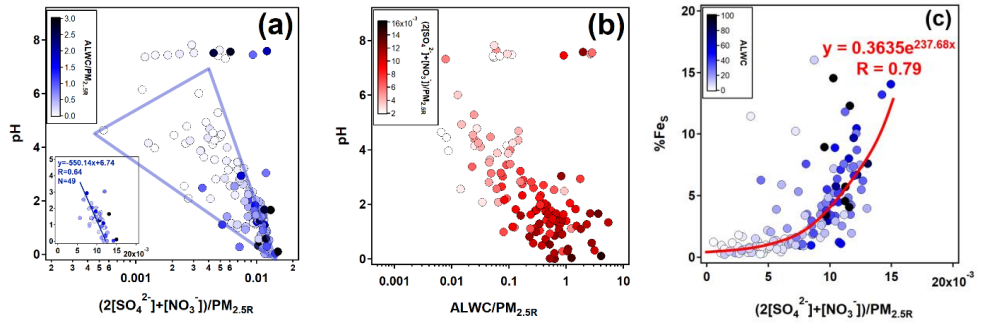

Figure 3: Relationships among pH, relative abundance (unit: µmol μg^{-1}, normalized to the reconstructed $PM_{2.5}$) of ALWC and main acidic species (= $2[SO_4^{2-}] + [NO_3^-]$) and %Fes. The subgraph at the bottom-left of picture (a) shows the relationship between pH and the relative content of acidic species during clean and SP periods. An extreme point (pH = 7.46) was removed to obtain the robust correlation coefficient. Circles in (c) are colored by ALWC (unit: µg m^{-3}).

There was no prominent correlation between pH and ALWC when the pH exceeded 6 (Figure 3b). When the pH was smaller than 6, the increasing ALWC facilitated the heterogeneous reactions of SO_2 and NO_2 to generate more SO_4^{2-} and NO_3^-, lowering the aerosol pH and enhancing the %Fes. The formation of sulfate and nitrate will further facilitate the growth of ALWC due to their remarkable hygroscopicity, establishing a positive feedback (Path A in Figure 4), referred to as the "ALWC-acid" feedback (Wang et al., 2016; Wu et al., 2018b). On the other hand, ALWC dilutes H^+ in aerosol water. This process weakens the aerosol acidity and inhibits the particles from %Fes elevation (Path B in Figure 4). In addition, the increasing ALWC served as a medium for loading water-soluble components may promote the formation of Fes (Path C in Figure 4). The profound influence of acidic species on the aerosol pH indicates the predominance of the "ALWC-acid" feedback in modulating the aerosol pH and augmenting %Fes (Figure 3a and 3c). The high %Fes we observed during daytime and nighttime can be attributed to the relatively higher content of acidic species in $PM_{2.5}$.

https://doi.org/10.5194/egusphere-2023-2698
Preprint. Discussion started: 6 December 2023
© Author(s) 2023. CC BY 4.0 License.

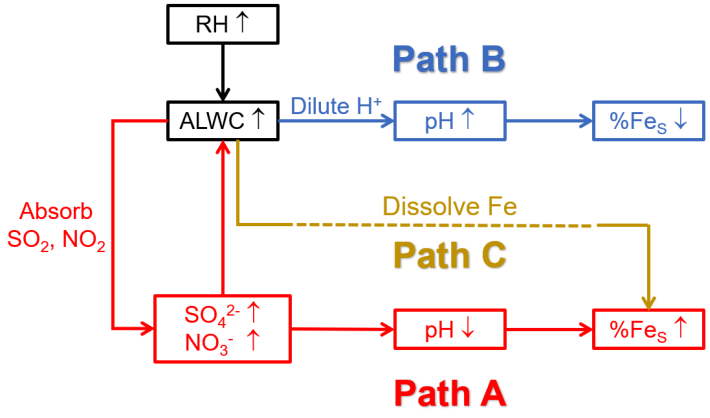

Figure 4: Schematic diagram of ALWC affecting pH and %Fes. Path C is challenging to observe and quantify because of the Fes extraction using MilliQ water in the sample pretreatment.

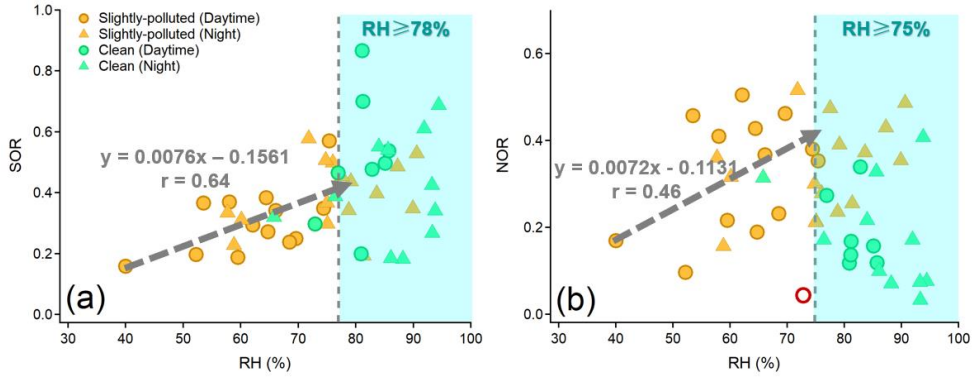

Figure 5: The dependence of SOR (a) and NOR (b) on RH during clean and slightly-polluted periods. The fitting of the regression line between SOR and RH was fitted when RH<78%. The fitting of the regression line between NOR and RH was fitted when RH<75% and one deviation point (the red circle in (b)) was removed.

RH is a key factor in the formation of SO_4^{2-} and NO_3^- through heterogeneous/aqueous-phase reactions within aerosols in Qingdao (Wang et al., 2016; Liu et al., 2020; Hou et al., 2022). The strong dependencies of the oxidation rate of sulfur (SOR, defined as $[SO_4^{2-}]/([SO_4^{2-}]+[SO_2])$ and nitrogen (NOR, defined as $[NO_3^-]/([NO_3^-]+[NO_2])$ on RH were observed under moderate humid conditions (RH≤75%). A decrease of 10% in RH resulted in a notable reduction of 7.6% in SOR and 7.2% in NOR (Figure 5). Such pronounced RH-dependencies were predominantly

https://doi.org/10.5194/egusphere-2023-2698
Preprint. Discussion started: 6 December 2023
© Author(s) 2023. CC BY 4.0 License.

observed during the nighttime of the SP period, indicating the significant role of heterogeneous reactions in controlling the formation of SO_4^{2-} and NO_3^-. The facilitation of aqueous-phase conversions leading to the formation of SO_4^{2-} and NO_3^- was more pronounced at night during the SP period, attributed to high RH. This, in turn, resulted in elevated SOR and a large fraction of SO_4^{2-} (Figures 2b and S2). The nighttime aerosol pH was approximately 0.16 units lower than that during daytime, but this slight variation did not hinder the efficient formation of Fe_S during nighttime in SP periods.

In contrast, during the daytime and nighttime in clean periods, RH was generally above 80%. The SOR was 0.49 on average and did not exhibit a clear correlation with RH beyond 78% (Figure 5a). Similar phenomena have been observed in previous studies, suggesting the existence of a saturation point in the promotion of RH on the aqueous-phase formation of SO_4^{2-} (Wang et al., 2019; Wang et al., 2021). High RH (> 70%) can cause water-soluble species to deliquesce and form an aqueous layer on the particle surface. Once the aqueous layer forms, the influence of RH variations becomes small (Shi et al., 2022). Consequently, the extent of aqueous-phase conversions promoting SO_4^{2-} formation during daytime in clean periods was comparable to that during nighttime.

4.2 Daytime enhancement by photocatalysis reactions

Photochemical reactions can enhance the formation of acidic species and increase the aerosol $\%Fe_S$ through aerosol acidification (Tao et al., 2020; Liu et al., 2021a). The large proportion of acidic species during the daytime of the clean period was attributable to SO_4^{2-}, which was 6.1% higher than the nighttime SO_4^{2-} (Figures 2a and 2b). Although the level of SO_2 during daytime was similar to that observed during nighttime, the daytime SOR was as high as 0.50 ± 0.20 (Figure S2). The rates of aqueous-phase conversion were similar during daytime and nighttime during the clean period. Therefore, the substantial fraction of SO_4^{2-} was most likely caused by photochemical reactions.

O_x (described by the sum of O_3 and NO_2) was investigated to quantify the potential of photochemical reactions, following the method of Wu et al. (2018a). The daytime O_x concentration (56.1 ± 6.4 ppb) was about 5.1% higher than that of nighttime O_x (53.4 ± 9.3 ppb) during the clean period. The substantial SOR occurred under the extreme O_x conditions (Figure 6a), suggesting a substantial contribution of the photochemical reactions during the clean period. Moreover, there was a significant correlation (r = 0.82) between $\%Fe_S$ and the molar ratio of [oxalate]/[Fe_T] during daytime (Figure 7a). Oxalate can form complexes with Fe(III) and engage in photochemical reactions through photo-induced charge transfer. Oxalate transfers its charge to the Fe(III) surface, resulting in the reduction

https://doi.org/10.5194/egusphere-2023-2698
Preprint. Discussion started: 6 December 2023
© Author(s) 2023. CC BY 4.0 License.

of Fe(III) to Fe(II), followed by the dissociation of the formed Fe(II) from the surface and hence the dissolution of aerosol Fe (Zuo and Hoigne, 1992; Zhang et al., 2019; Lueder et al., 2020). Shi et al. (2022) validated the outstanding performance of the ratio of oxalate/Fe_T in predicting the aerosol %Fe_S. This finding guarantees a further investigation of the correlation between aerosol %Fe_S and acidities. As shown in Figure S3a and S3b, the slope of the regression line of between Fe_S and oxalate was much higher during daytime (k = 146.4) than that during nighttime (k = 21.6), indicating that oxalate promoted the dissolution of aerosol Fe via Fe-oxalate complexes related photochemistry (Zhou et al., 2020). These results demonstrate that the enhancement of daytime photochemistry and aqueous chemistry on aerosol %Fe_S was more pronounced than that of the nighttime aqueous reactions during the clean period (Figure 8a and 8b).

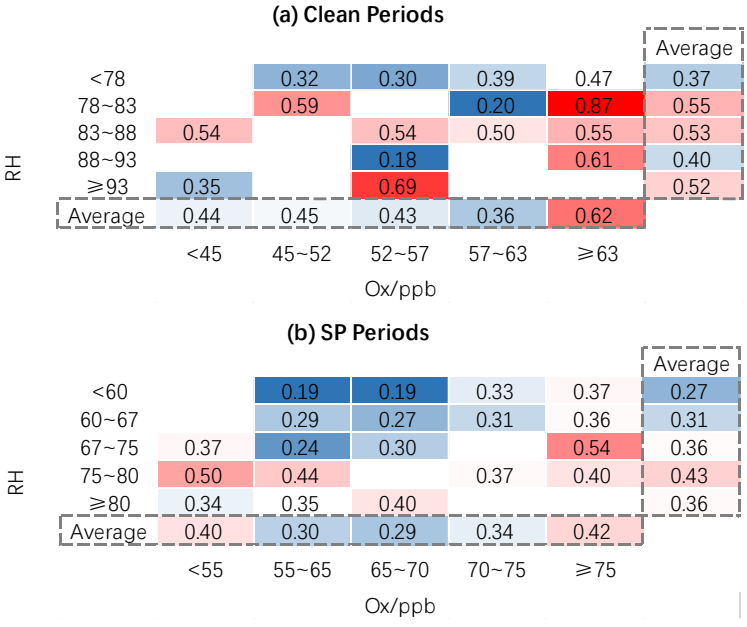

Figure 6: RH-O_x image plots colored by SOR during clean and SP periods.

During the SP period, the extent of SOR was more influenced by RH than by O_x, particularly when RH was below 80% (Figure 6b). Nighttime SOR (0.37 ± 0.12) was approximately 1.2 times higher than the daytime SOR (0.31 ± 0.11) even though the daytime O_x concentration was larger than that during nighttime (Figure S2), indicating more

https://doi.org/10.5194/egusphere-2023-2698
Preprint. Discussion started: 6 December 2023
© Author(s) 2023. CC BY 4.0 License.

contribution of liquid/heterogeneous reactions to the SO_4^{2-} formation than photocatalysis reactions. Similar findings were reported by Hou et al. (2022), who highlighted the dominant role of humidity rather than O_x in SO_4^{2-} formation in haze intensification.

In summary, the nighttime exhibited a stronger "ALWC-acid" feedback compared to the daytime during the SP period. The influence of the combination of daytime photochemistry and aqueous-phase reactions was comparatively weaker than nighttime aqueous chemistry, so the nighttime $\%Fe_S$ was higher than the daytime $\%Fe_S$ (Figure 8c and 8d). It is noteworthy that O_x concentration was significantly higher during the SP period compared to the clean period (Figure S2), suggesting more active daytime photocatalysis reactions during the SP period. However, the impact of aqueous-phase conversions during the SP nighttime period was relatively weak compared to the nighttime of clean periods. These results imply that the role of photocatalysis reactions in SO_4^{2-} formation, and subsequently in the elevation of aerosol $\%Fe_S$, was feeble compared to aqueous-phase conversions.

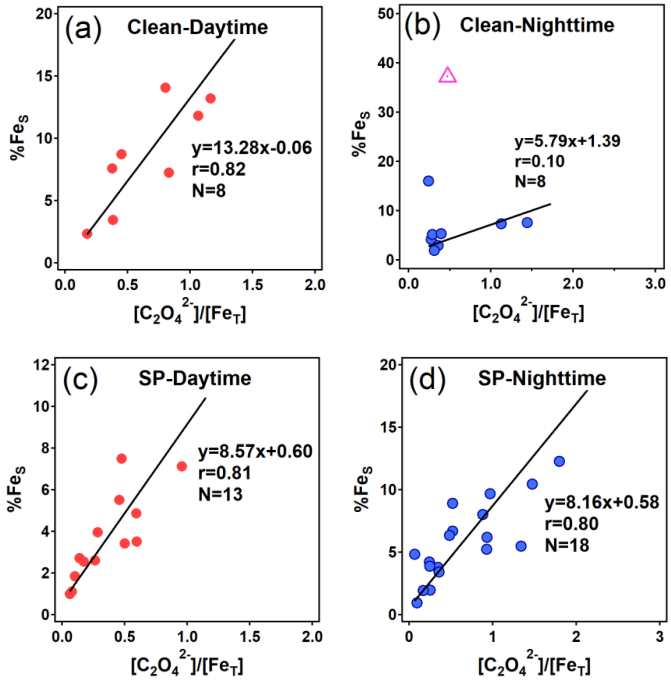

Figure 7: Relationships between $\%Fe_S$ and the molar ratio (unit: μmol μmol^{-1}) of oxalate to Fe_T during daytime and nighttime in clean and SP periods. An extreme point (marked by a pink triangle, $\%Fe_S$ = 37.2%) in (b) was removed to obtain a more robust correlation coefficient.

https://doi.org/10.5194/egusphere-2023-2698
Preprint. Discussion started: 6 December 2023
© Author(s) 2023. CC BY 4.0 License.

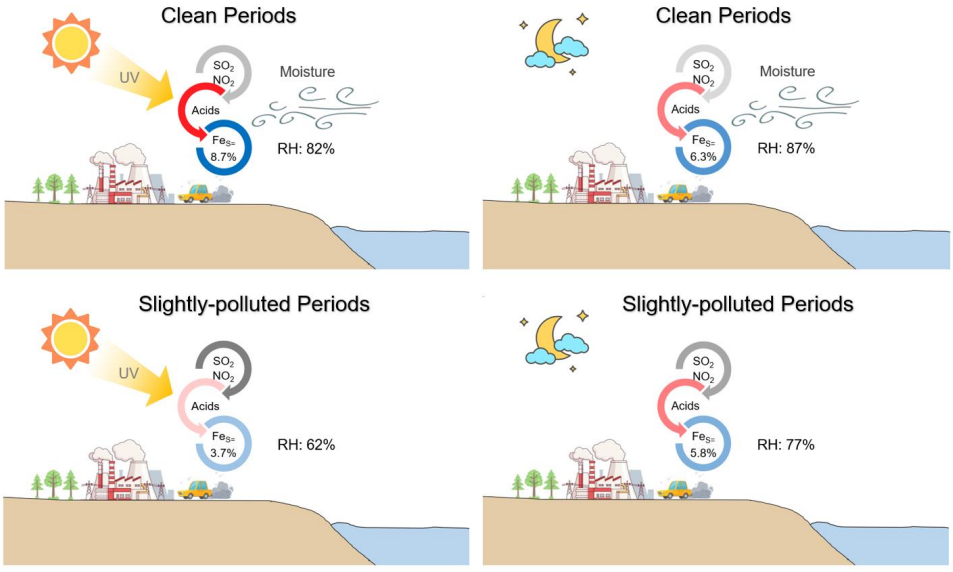

Figure 8: Conceptual diagram showing the Fe dissolution influenced by acid processes at the coastal city during daytime and nighttime in clean and SP periods.

Enhancing aerosol %Fe_S through direct photocatalysis pathways is indeed possible. Iron oxides in minerals can generate conduction band electrons upon irradiation, causing the reductive dissolution of Fe(III)-containing solid phases to Fe(II) species (Zhang et al., 1993; Fu et al., 2010). However, structural Fe(III), which is the major iron-related mineral in dust and coal fly ash, does not readily undergo direct reduction upon UV irradiation (Fu et al., 2012; Fu et al., 2010; Xie et al., 2020). Another pathway for photolysis-conduced iron dissolution involves the reduction by reactive oxygen species (ROS, e.g., $O_2^{\bullet-}$, $HO_2^{\bullet}$, and H_2O_2). These ROS may be generated from dissolved oxygen accompanied by conduction band electrons, enhancing the Fe dissolution by reducing the solid-phase Fe(III) into the more soluble Fe(II) form (Zhu et al., 1997; Hettiarachchi and Rubasinghege, 2020). Aerosol water is necessary for the above reactions, and the proton-promoted dissolution by acid species is indispensable to dissolve the solid-phase Fe(II) into aerosol solutions. We suppose that the observed weak influence of photocatalysis on %Fe_S was because of the extreme aerosol acidity. The acidity of aerosols, such as a pH as low as 2.0 during daytime of the present study, can suppress the contribution of photochemical catalysis in the formation of Fe_S (Zhu et al., 1993; Fu et al., 2010; Fu et al., 2012). In addition, studies have suggested that Fe dissolution can be inhibited in H_2SO_4 systems under irradiation compared to dark conditions, which could be

https://doi.org/10.5194/egusphere-2023-2698
Preprint. Discussion started: 6 December 2023
© Author(s) 2023. CC BY 4.0 License.

another reason for the low %Fe_S during daytime although the exact mechanism remains unclear (Fu et al., 2010; Hettiarachchi et al., 2018).

4.3 Environmental implications

Limited research has been conducted on the diurnal variation of aerosol %Fe_S. Only an early case investigated the diel variability of Fe species at an island located in the Caribbean Sea and studied the photochemical processing of Fe (Zhu et al., 1997). A strong correlation between Fe_S and acid species at aerosol pH of 0−1 was reported, suggesting the great influence of aerosol acidification on Fe dissolution. These findings align with the results of our study. Our results suggest that aqueous-phase conversions promoted by acid processes can play a more significant role in modifying aerosol %Fe_S compared to photochemical reactions under specific conditions in coastal cities.

Previous studies pinpointed robust %Fe_S of anthropogenic aerosols, especially for combustion-related fly ash (Oakes et al., 2012; Wang et al., 2015; Baldo et al., 2022; Li et al., 2022). Unlike urban air, RH is often very high over the open ocean, leading to more widespread promotion of heterogeneous reactions and the secondary formation of SO_4^{2-} and NO_3^-. In such cases, photochemical reactions and precursors' concentrations will determine the salt formation. Given the air mass of the clean period was a mixture of marine air and the local urban air, it is expected that the Fe dissolution in aerosol particles is an effective way to produce Fe_S during daytime. Air masses transported from the land-populated areas carry substantial amounts of SO_2, NO_2 and NH_3 to offshore areas, facilitate the formation of SO_4^{2-} and NO_3^- and conduce to the acidic dissolution of Fe in aerosol particles. Then, the solubilized Fe_S through proton-promoted dissolution can be further stabilized by the organic complexation of Fe in the marine atmosphere (Sakata et al., 2022).

Additionally, the dearth of ammonia sources in the marine atmosphere may impede the formation of SO_4^{2-} and NO_3^- to some extent on the one hand (Wang et al., 2017; Guo et al., 2018). The scarceness of ammonia may be also conducive to enhancing the aerosol acidity and elevating aerosol %Fe_S on the other hand. Given that the HCl concentration in remote marine atmospheric boundary layer is typically higher than in the continent of East Asia, the influence of chloride on aerosol pH may therefore play a conspicuous role in regulating %Fe_S (Tobo et al., 2010), on which knowledge is very limited.

https://doi.org/10.5194/egusphere-2023-2698
Preprint. Discussion started: 6 December 2023
© Author(s) 2023. CC BY 4.0 License.

5 Summary

This study investigated the daytime and nighttime $\%Fe_S$ in $PM_{2.5}$ in a coastal city of China under clean and SP conditions. Under clean conditions, $\%Fe_S$ was higher during daytime (8.7%) compared to the nighttime (6.3%, after removing an extreme point of 37.2%). On the contrary, under SP conditions, $\%Fe_S$ was higher at night (5.8%) than during daytime (3.7%). Significant correlations were observed between the main acidic components (SO_4^{2-} and NO_3^-), aerosol pH, and $\%Fe_S$, indicating that the acid process played a dominant role in influencing aerosol $\%Fe_S$.

The RH consistently exceeded 80% during both daytime and nighttime in clean periods. Aqueous-phase reactions were found to be most effective in promoting the secondary formation of acid species, with photochemical processes further enhancing SO_4^{2-} formation during daytime. Together with the lower ALWC, the aerosol pH was much lower during daytime (0.54 ± 0.81) compared to nighttime (1.20 ± 0.89) during the clean period, which exerted a more significant influence on aerosol Fe dissolution. In contrast, RH was much higher at night (76.7%) than that during daytime (62.8%) in SP periods. The dry conditions during daytime notably restricted the secondary formation of SO_4^{2-} and NO_3^-. The acid content in $PM_{2.5}$ was much higher at night under the promotion of heterogeneous processes, resulting in stronger aerosol acidity and higher aerosol $\%Fe_S$.

This study provides insights into the mechanisms of aerosol $\%Fe_S$ modulation in the coastal city. The robust promotion of aqueous-phase processes and the comparatively weaker influence of photochemistry on enhancing aerosol $\%Fe_S$ were observed. In urban air, RH was a crucial factor in controlling $\%Fe_S$ through modulating the heterogeneous reactions of SO_4^{2-} and NO_3^-. In contrast, in the oceanic atmospheric boundary layer, precursors' levels and photochemical processes may be the decisive manipulators on aerosol $\%Fe_S$. Therefore, the content of bioavailable Fe in urban-related aerosols may be greatly elevated after intrusion into the marine atmosphere, which holds significant importance for future research.

Author contributions. *WL: investigation, formal analysis, writing – original draft, writing – review and editing; YQ: methodology; YL: methodology; GW: visualization; YZ: methodology; JS: methodology; WQ: methodology; LS: supervision, funding acquisition; WW: methodology; DZ: funding acquisition, methodology, writing – review and editing; YZ: conceptualization, funding acquisition, methodology, supervision, writing – review and editing.*

Competing interests. *The authors declare that they have no conflict of interests.*

https://doi.org/10.5194/egusphere-2023-2698
Preprint. Discussion started: 6 December 2023
© Author(s) 2023. CC BY 4.0 License.

Financial support. *This research was supported by National Natural Science Foundation of China (Grant Number: 41875155, 41605114, 41875174) and the Overseas Joint Training Program for Doctoral Students of Ocean University of China. D.Z. was supported by JSPS KAKENHI 21H01158.*

References

Arimoto, R., Zhang, X. Y., Huebert, B. J., Kang, C. H., Savoie, D. L., Prospero, J. M., Sage, S. K., Schloesslin, C. A., Khaing, H. M., and Oh, S. N.: Chemical composition of atmospheric aerosols from Zhenbeitai, China, and Gosan, South Korea, during ACE-Asia, Journal of Geophysical Research: Atmospheres, 109, 10.1029/2003JD004323, 2004.

Baldo, C., Ito, A., Krom, M. D., Li, W., Jones, T., Drake, N., Ignatyev, K., Davidson, N., and Shi, Z.: Iron from coal combustion particles dissolves much faster than mineral dust under simulated atmospheric acidic conditions, Atmos. Chem. Phys., 22, 6045–6066, 10.5194/acp-22-6045-2022, 2022.

Chen, H. and Grassian, V. H.: Iron Dissolution of Dust Source Materials during Simulated Acidic Processing: The Effect of Sulfuric, Acetic, and Oxalic Acids, Environ. Sci. Technol., 47, 10312–10321, 10.1021/es401285s, 2013.

Chen, Y. and Siefert, R. L.: Seasonal and spatial distributions and dry deposition fluxes of atmospheric total and labile iron over the tropical and subtropical North Atlantic Ocean, Journal of Geophysical Research: Atmospheres, 109, https://doi.org/10.1029/2003JD003958, 2004.

Fu, H., Cwiertny, D. M., Carmichael, G. R., Scherer, M. M., and Grassian, V. H.: Photoreductive dissolution of Fe-containing mineral dust particles in acidic media, Journal of Geophysical Research: Atmospheres, 115, https://doi.org/10.1029/2009JD012702, 2010.

Fu, H., Lin, J., Shang, G., Dong, W., Grassian, V. H., Carmichael, G. R., Li, Y., and Chen, J.: Solubility of Iron from Combustion Source Particles in Acidic Media Linked to Iron Speciation, Environ. Sci. Technol., 46, 11119–11127, 10.1021/es302558m, 2012.

Guo, H., Otjes, R., Schlag, P., Kiendler-Scharr, A., Nenes, A., and Weber, R. J.: Effectiveness of ammonia reduction on control of fine particle nitrate, Atmos. Chem. Phys., 18, 12241–12256, 10.5194/acp-18-12241-2018, 2018.

Hennigan, C. J., Izumi, J., Sullivan, A. P., Weber, R. J., and Nenes, A.: A critical evaluation of proxy methods used to estimate the acidity of atmospheric particles, Atmos. Chem. Phys., 15, 2775–2790, 10.5194/acp-15-2775-2015, 2015.

Hettiarachchi, E. and Rubasinghege, G.: Mechanistic Study on Iron Solubility in Atmospheric Mineral Dust Aerosol: Roles of Titanium, Dissolved Oxygen, and Solar Flux in Solutions Containing Different Acid Anions, ACS Earth and Space Chemistry, 4, 101–111, 10.1021/acsearthspacechem.9b00280, 2020.

Hettiarachchi, E., Hurab, O., and Rubasinghege, G.: Atmospheric Processing and Iron Mobilization of Ilmenite: Iron-Containing Ternary Oxide in Mineral Dust Aerosol, The Journal of Physical Chemistry A, 122, 1291–1302, 10.1021/acs.jpca.7b11320, 2018.

Hettiarachchi, E., Reynolds, R. L., Goldstein, H. L., Moskowitz, B., and Rubasinghege, G.: Bioavailable iron production in airborne mineral dust: Controls by chemical composition and solar flux, Atmos. Environ., 205, 90–102, https://doi.org/10.1016/j.atmosenv.2019.02.037, 2019.

Hou, L., Dai, Q., Song, C., Liu, B., Guo, F., Dai, T., Li, L., Liu, B., Bi, X., Zhang, Y., and Feng, Y.: Revealing Drivers of Haze Pollution by Explainable Machine Learning, Environmental Science & Technology Letters, 9, 112–119, 10.1021/acs.estlett.1c00865, 2022.

https://doi.org/10.5194/egusphere-2023-2698
Preprint. Discussion started: 6 December 2023
© Author(s) 2023. CC BY 4.0 License.

Huang, K., Zhuang, G., Li, J., Wang, Q., Sun, Y., Lin, Y., and Fu, J. S.: Mixing of Asian dust with pollution aerosol and the transformation of aerosol components during the dust storm over China in spring 2007, Journal of Geophysical Research: Atmospheres, 115, 10.1029/2009JD013145, 2010.

Li, K., Fang, X., Wang, T., Gong, K., Ali Tahir, M., Wang, W., Han, J., Cheng, H., Xu, G., and Zhang, L.: Atmospheric organic complexation enhanced sulfate formation and iron dissolution on nano α-Fe2O3, Environmental Science: Nano, 8, 698–710, 10.1039/D0EN01220C, 2021.

Li, R., Zhang, H., Wang, F., He, Y., Huang, C., Luo, L., Dong, S., Jia, X., and Tang, M.: Mass fractions, solubility, speciation and isotopic compositions of iron in coal and municipal waste fly ash, Science of The Total Environment, 838, 155974, https://doi.org/10.1016/j.scitotenv.2022.155974, 2022.

Li, W., Qi, Y., Qu, W., Qu, W., Shi, J., Zhang, D., Liu, Y., Zhang, Y., Zhang, W., Ren, D., Ma, Y., Wang, X., Yi, L., Sheng, L., and Zhou, Y.: PM2.5 source apportionment identified with total and soluble elements in positive matrix factorization, Sci. Total Environ., 858, 159948, https://doi.org/10.1016/j.scitotenv.2022.159948, 2023a.

Li, W., Qi, Y., Qu, W., Qu, W., Shi, J., Zhang, D., Liu, Y., Wu, F., Ma, Y., Zhang, Y., Ren, D., Du, X., Yang, S., Wang, X., Yi, L., Gao, X., Wang, W., Ma, Y., Sheng, L., and Zhou, Y.: Sulfate and nitrate elevation in reverse-transport dust plumes over coastal areas of China, Atmos. Environ., 295, 119518, https://doi.org/10.1016/j.atmosenv.2022.119518, 2023b.

Liu, L., Lin, Q., Liang, Z., Du, R., Zhang, G., Zhu, Y., Qi, B., Zhou, S., and Li, W.: Variations in concentration and solubility of iron in atmospheric fine particles during the COVID-19 pandemic: An example from China, Gondwana Research, 97, 138–144, https://doi.org/10.1016/j.gr.2021.05.022, 2021a.

Liu, P., Ye, C., Xue, C., Zhang, C., Mu, Y., and Sun, X.: Formation mechanisms of atmospheric nitrate and sulfate during the winter haze pollution periods in Beijing: gas-phase, heterogeneous and aqueous-phase chemistry, Atmos. Chem. Phys., 20, 4153–4165, 10.5194/acp-20-4153-2020, 2020.

Liu, T., Chan, A. W. H., and Abbatt, J. P. D.: Multiphase Oxidation of Sulfur Dioxide in Aerosol Particles: Implications for Sulfate Formation in Polluted Environments, Environ. Sci. Technol., 55, 4227–4242, 10.1021/acs.est.0c06496, 2021b.

Lueder, U., Jørgensen, B. B., Kappler, A., and Schmidt, C.: Photochemistry of iron in aquatic environments, Environmental Science: Processes & Impacts, 22, 12–24, 10.1039/C9EM00415G, 2020.

Martin, J. H., Coale, K. H., Johnson, K. S., Fitzwater, S. E., Gordon, R. M., Tanner, S. J., Hunter, C. N., Elrod, V. A., Nowicki, J. L., Coley, T. L., Barber, R. T., Lindley, S., Watson, A. J., Van Scoy, K., Law, C. S., Liddicoat, M. I., Ling, R., Stanton, T., Stockel, J., Collins, C., Anderson, A., Bidigare, R., Ondrusek, M., Latasa, M., Millero, F. J., Lee, K., Yao, W., Zhang, J. Z., Friederich, G., Sakamoto, C., Chavez, F., Buck, K., Kolber, Z., Greene, R., Falkowski, P., Chisholm, S. W., Hoge, F., Swift, R., Yungel, J., Turner, S., Nightingale, P., Hatton, A., Liss, P., and Tindale, N. W.: Testing the iron hypothesis in ecosystems of the equatorial Pacific Ocean, Nature, 371, 123–129, 10.1038/371123a0, 1994.

Oakes, M., Ingall, E. D., Lai, B., Shafer, M. M., Hays, M. D., Liu, Z. G., Russell, A. G., and Weber, R. J.: Iron Solubility Related to Particle Sulfur Content in Source Emission and Ambient Fine Particles, Environ. Sci. Technol., 46, 6637–6644, 10.1021/es300701c, 2012.

Pang, H., Zhang, Q., Wang, H., Cai, D., Ma, Y., Li, L., Li, K., Lu, X., Chen, H., Yang, X., and Chen, J.: Photochemical Aging of Guaiacol by Fe(III)–Oxalate Complexes in Atmospheric Aqueous Phase, Environ. Sci. Technol., 53, 127–136, 10.1021/acs.est.8b04507, 2019.

Pye, H. O. T., Nenes, A., Alexander, B., Ault, A. P., Barth, M. C., Clegg, S. L., Collett Jr, J. L., Fahey, K. M., Hennigan, C. J., Herrmann, H., Kanakidou, M., Kelly, J. T., Ku, I. T., McNeill, V. F., Riemer, N., Schaefer,

https://doi.org/10.5194/egusphere-2023-2698
Preprint. Discussion started: 6 December 2023
© Author(s) 2023. CC BY 4.0 License.

T., Shi, G., Tilgner, A., Walker, J. T., Wang, T., Weber, R., Xing, J., Zaveri, R. A., and Zuend, A.: The acidity of atmospheric particles and clouds, Atmos. Chem. Phys., 20, 4809–4888, 10.5194/acp-20-4809-2020, 2020.

Sakata, K., Kurisu, M., Takeichi, Y., Sakaguchi, A., Tanimoto, H., Tamenori, Y., Matsuki, A., and Takahashi, Y.: Iron (Fe) speciation in size-fractionated aerosol particles in the Pacific Ocean: The role of organic complexation of Fe with humic-like substances in controlling Fe solubility, Atmos. Chem. Phys., 22, 9461–9482, 10.5194/acp-22-9461-2022, 2022.

Shi, J.-H., Zhang, J., Gao, H.-W., Tan, S.-C., Yao, X.-H., and Ren, J.-L.: Concentration, solubility and deposition flux of atmospheric particulate nutrients over the Yellow Sea, Deep Sea Research Part II: Topical Studies in Oceanography, 97, 43–50, https://doi.org/10.1016/j.dsr2.2013.05.004, 2013.

Shi, J., Guan, Y., Gao, H., Yao, X., Wang, R., and Zhang, D.: Aerosol Iron Solubility Specification in the Global Marine Atmosphere with Machine Learning, Environ. Sci. Technol., 56, 16453–16461, 10.1021/acs.est.2c05266, 2022.

Shi, J., Guan, Y., Ito, A., Gao, H., Yao, X., Baker, A. R., and Zhang, D.: High Production of Soluble Iron Promoted by Aerosol Acidification in Fog, Geophys. Res. Lett., 47, e2019GL086124, https://doi.org/10.1029/2019GL086124, 2020.

Shi, Z., Krom, M. D., Jickells, T. D., Bonneville, S., Carslaw, K. S., Mihalopoulos, N., Baker, A. R., and Benning, L. G.: Impacts on iron solubility in the mineral dust by processes in the source region and the atmosphere: A review, Aeolian Research, 5, 21–42, https://doi.org/10.1016/j.aeolia.2012.03.001, 2012.

Shi, Z. B., Krom, M. D., Bonneville, S., and Benning, L. G.: Atmospheric Processing Outside Clouds Increases Soluble Iron in Mineral Dust, Environ. Sci. Technol., 49, 1472–1477, 10.1021/es504623x, 2015.

Solmon, F., Chuang, P. Y., Meskhidze, N., and Chen, Y.: Acidic processing of mineral dust iron by anthropogenic compounds over the north Pacific Ocean, Journal of Geophysical Research: Atmospheres, 114, https://doi.org/10.1029/2008JD010417, 2009.

Song, S., Gao, M., Xu, W., Shao, J., Shi, G., Wang, S., Wang, Y., Sun, Y., and McElroy, M. B.: Fine-particle pH for Beijing winter haze as inferred from different thermodynamic equilibrium models, Atmos. Chem. Phys., 18, 7423–7438, 10.5194/acp-18-7423-2018, 2018.

Sorooshian, A., Wang, Z., Coggon, M. M., Jonsson, H. H., and Ervens, B.: Observations of Sharp Oxalate Reductions in Stratocumulus Clouds at Variable Altitudes: Organic Acid and Metal Measurements During the 2011 E-PEACE Campaign, Environ. Sci. Technol., 47, 7747–7756, 10.1021/es4012383, 2013.

Sugie, K., Nishioka, J., Kuma, K., Volkov, Y. N., and Nakatsuka, T.: Availability of particulate Fe to phytoplankton in the Sea of Okhotsk, Mar. Chem., 152, 20–31, https://doi.org/10.1016/j.marchem.2013.03.005, 2013.

Tao, W., Su, H., Zheng, G., Wang, J., Wei, C., Liu, L., Ma, N., Li, M., Zhang, Q., Pöschl, U., and Cheng, Y.: Aerosol pH and chemical regimes of sulfate formation in aerosol water during winter haze in the North China Plain, Atmos. Chem. Phys., 20, 11729–11746, 10.5194/acp-20-11729-2020, 2020.

Tobo, Y., Zhang, D., Matsuki, A., and Iwasaka, Y.: Asian dust particles converted into aqueous droplets under remote marine atmospheric conditions, Proc. Natl. Acad. Sci. U.S.A., 107, 17905, 2010.

Turpin, B. J. and Lim, H.-J.: Species Contributions to PM2.5 Mass Concentrations: Revisiting Common Assumptions for Estimating Organic Mass, Aerosol Science and Technology, 35, 602–610, 10.1080/02786820119445, 2001.

Wang, G., Zhang, R., Gomez, M. E., Yang, L., Zamora, M. L., Hu, M., Lin, Y., Peng, J., Guo, S., Meng, J., Li, J., Cheng, C., Hu, T., Ren, Y., Wang, Y., Gao, J., Cao, J., An, Z., Zhou, W., Li, G., Wang, J., Tian, P., Marrero-Ortiz, W., Secrest, J., Du, Z., Zheng, J., Shang, D., Zeng, L., Shao, M., Wang, W., Huang, Y., Wang, Y., Zhu, Y., Li, Y., Hu, J., Pan, B., Cai, L., Cheng, Y., Ji, Y., Zhang, F., Rosenfeld, D., Liss, P. S., Duce, R. A., Kolb, C.

https://doi.org/10.5194/egusphere-2023-2698
Preprint. Discussion started: 6 December 2023
© Author(s) 2023. CC BY 4.0 License.

E., and Molina, M. J.: Persistent sulfate formation from London Fog to Chinese haze, Proc. Natl. Acad. Sci. U.S.A., 113, 13630, 2016.

Wang, J., Zhao, B., Wang, S., Yang, F., Xing, J., Morawska, L., Ding, A., Kulmala, M., Kerminen, V.-M., Kujansuu, J., Wang, Z., Ding, D., Zhang, X., Wang, H., Tian, M., Petäjä, T., Jiang, J., and Hao, J.: Particulate matter pollution over China and the effects of control policies, Science of The Total Environment, 584–585, 426–447, https://doi.org/10.1016/j.scitotenv.2017.01.027, 2017.

Wang, Q., Zhuang, G., Li, J., Huang, K., Zhang, R., Jiang, Y., Lin, Y., and Fu, J. S.: Mixing of dust with pollution on the transport path of Asian dust - Revealed from the aerosol over Yulin, the north edge of Loess Plateau, Sci. Total Environ., 409, 573, 2011.

Wang, R., Balkanski, Y., Boucher, O., Bopp, L., Chappell, A., Ciais, P., Hauglustaine, D., Peñuelas, J., and Tao, S.: Sources, transport and deposition of iron in the global atmosphere, Atmos. Chem. Phys., 15, 6247–6270, 10.5194/acp-15-6247-2015, 2015.

Wang, X., Wei, W., Cheng, S., Zhang, H., and Yao, S.: Source estimation of SO_4^{2-} and NO_3^- based on monitoring-modeling approach during winter and summer seasons in Beijing and Tangshan, China, Atmos. Environ., 214, 116849, https://doi.org/10.1016/j.atmosenv.2019.116849, 2019.

Wang, Y., Hu, M., Hu, W., Zheng, J., Niu, H., Fang, X., Xu, N., Wu, Z., Guo, S., Wu, Y., Chen, W., Lu, S., Shao, M., Xie, S., Luo, B., and Zhang, Y.: Secondary Formation of Aerosols Under Typical High-Humidity Conditions in Wintertime Sichuan Basin, China: A Contrast to the North China Plain, J. Phys. Chem. A, 126, e2021JD034560, https://doi.org/10.1029/2021JD034560, 2021.

Watson, A. J. and Lefévre, N.: The sensitivity of atmospheric CO2 concentrations to input of iron to the oceans, Tellus B: Chemical and Physical Meteorology, 51, 453–460, 10.3402/tellusb.v51i2.16320, 1999.

Watson, A. J., Law, C. S., Van Scoy, K. A., Millero, F. J., Yao, W., Friederich, G. E., Liddicoat, M. I., Wanninkhof, R. H., Barber, R. T., and Coale, K. H.: Minimal effect of iron fertilization on sea-surface carbon dioxide concentrations, Nature, 371, 143–145, 10.1038/371143a0, 1994.

Weller, C., Tilgner, A., Bräuer, P., and Herrmann, H.: Modeling the Impact of Iron–Carboxylate Photochemistry on Radical Budget and Carboxylate Degradation in Cloud Droplets and Particles, Environ. Sci. Technol., 48, 5652–5659, 10.1021/es4056643, 2014.

Wong, J. P. S., Yang, Y., Fang, T., Mulholland, J. A., Russell, A. G., Ebelt, S., Nenes, A., and Weber, R. J.: Fine Particle Iron in Soils and Road Dust Is Modulated by Coal-Fired Power Plant Sulfur, Environ. Sci. Technol., 54, 7088–7096, 10.1021/acs.est.0c00483, 2020.

Wu, Y., Ge, X., Wang, J., Shen, Y., Ye, Z., Ge, S., Wu, Y., Yu, H., and Chen, M.: Responses of secondary aerosols to relative humidity and photochemical activities in an industrialized environment during late winter, Atmos. Environ., 193, 66–78, https://doi.org/10.1016/j.atmosenv.2018.09.008, 2018a.

Wu, Z., Wang, Y., Tan, T., Zhu, Y., Li, M., Shang, D., Wang, H., Lu, K., Guo, S., Zeng, L., and Zhang, Y.: Aerosol Liquid Water Driven by Anthropogenic Inorganic Salts: Implying Its Key Role in Haze Formation over the North China Plain, Environmental Science & Technology Letters, 5, 160–166, 10.1021/acs.estlett.8b00021, 2018b.

Xie, T., Lu, S., Zeng, J., Rao, L., Wang, X., Win, M. S., Zhang, D., Lu, H., Liu, X., and Wang, Q.: Soluble Fe release from iron-bearing clay mineral particles in acid environment and their oxidative potential, Science of The Total Environment, 726, 138650, https://doi.org/10.1016/j.scitotenv.2020.138650, 2020.

Yang, T., Chen, Y., Zhou, S., Li, H., Wang, F., and Zhu, Y.: Solubilities and deposition fluxes of atmospheric Fe and Cu over the Northwest Pacific and its marginal seas, Atmos. Environ., 239, 117763, https://doi.org/10.1016/j.atmosenv.2020.117763, 2020.

https://doi.org/10.5194/egusphere-2023-2698
Preprint. Discussion started: 6 December 2023
© Author(s) 2023. CC BY 4.0 License.

Zhang, G., Lin, Q., Peng, L., Yang, Y., Jiang, F., Liu, F., Song, W., Chen, D., Cai, Z., Bi, X., Miller, M., Tang, M., Huang, W., Wang, X., Peng, P. a., and Sheng, G.: Oxalate Formation Enhanced by Fe-Containing Particles and Environmental Implications, Environ. Sci. Technol., 53, 1269–1277, 10.1021/acs.est.8b05280, 2019.

Zhang, H., Li, R., Dong, S., Wang, F., Zhu, Y., Meng, H., Huang, C., Ren, Y., Wang, X., Hu, X., Li, T., Peng, C., Zhang, G., Xue, L., Wang, X., and Tang, M.: Abundance and Fractional Solubility of Aerosol Iron During Winter at a Coastal City in Northern China: Similarities and Contrasts Between Fine and Coarse Particles, Journal of Geophysical Research: Atmospheres, 127, e2021JD036070, https://doi.org/10.1029/2021JD036070, 2022.

Zhang, Z., Boxall, C., and Kelsall, G. H.: Photoelectrophoresis of colloidal iron oxides 1. Hematite (α-Fe2O3), in: Colloids in the Aquatic Environment, edited by: Tadros, T. F., and Gregory, J., Elsevier, Oxford, 145–163, https://doi.org/10.1016/B978-1-85861-038-2.50014-0, 1993.

Zhou, Y., Zhang, Y., Griffith, S. M., Wu, G., Li, L., Zhao, Y., Li, M., Zhou, Z., and Yu, J. Z.: Field Evidence of Fe-Mediated Photochemical Degradation of Oxalate and Subsequent Sulfate Formation Observed by Single Particle Mass Spectrometry, Environ. Sci. Technol., 54, 6562–6574, 10.1021/acs.est.0c00443, 2020.

Zhu, X., Prospero, J. M., Savoie, D. L., Millero, F. J., Zika, R. G., and Saltzman, E. S.: Photoreduction of iron(III) in marine mineral aerosol solutions, Journal of Geophysical Research: Atmospheres, 98, 9039–9046, https://doi.org/10.1029/93JD00202, 1993.

Zhu, X. R., Prospero, J. M., and Millero, F. J.: Diel variability of soluble Fe(II) and soluble total Fe in North African dust in the trade winds at Barbados, Journal of Geophysical Research: Atmospheres, 102, 21297–21305, https://doi.org/10.1029/97JD01313, 1997.

Zhu, Y., Li, W., Lin, Q., Yuan, Q., Liu, L., Zhang, J., Zhang, Y., Shao, L., Niu, H., Yang, S., and Shi, Z.: Iron solubility in fine particles associated with secondary acidic aerosols in east China, Environmental Pollution, 264, 114769, https://doi.org/10.1016/j.envpol.2020.114769, 2020.

Zhuang, G., Yi, Z., Duce, R. A., and Brown, P. R.: Link between iron and sulphur cycles suggested by detection of Fe(n) in remote marine aerosols, Nature, 355, 537–539, 10.1038/355537a0, 1992.

Zuo, Y. and Hoigne, J.: Formation of hydrogen peroxide and depletion of oxalic acid in atmospheric water by photolysis of iron(III)-oxalato complexes, Environ. Sci. Technol., 26, 1014–1022, 10.1021/es00029a022, 1992.